Calhoun: The NPS Institutional Archive

DSpace Repository

Faculty and Researchers | Faculty and Researchers' Publications

2020

Hidden Production: On the Importance of Pelagic Phytoplankton Blooms Beneath Arctic Sea Ice

Kinney, Jaclyn Clement; Maslowski, Wieslaw; Osinski, Robert; Jin, Meibing; Frants, Marina; Jeffery, Nicole; Lee, Younjoo J.

AGU

Clement Kinney, J., Maslowski, W., Osinski, R., Jin, M., Frants, M., Jeffery, N., & Lee, Y. J. (2020). Hidden production: On the importance of pelagic phytoplankton blooms beneath Arctic Sea ice. Journal of Geophysical Research: Oceans, 125, e2020JC016211. https://doi.org/10.1029/2020JC016211

http://hdl.handle.net/10945/66154

Downloaded from NPS Archive: Calhoun

http://www.nps.edu/library

Calhoun is the Naval Postgraduate School's public access digital repository for research materials and institutional publications created by the NPS community. Calhoun is named for Professor of Mathematics Guy K. Calhoun, NPS's first appointed -- and published -- scholarly author.

Dudley Knox Library / Naval Postgraduate School
411 Dyer Road / 1 University Circle
Monterey, California USA 93943

JGR Oceans

RESEARCH ARTICLE
10.1029/2020JC016211

Hidden Production: On the Importance of Pelagic Phytoplankton Blooms Beneath Arctic Sea Ice

Jaclyn Clement Kinney[1], Wieslaw Maslowski[1], Robert Osinski[2], Meibing Jin[3], Marina Frants[1], Nicole Jeffery[4], and Younjoo J. Lee[1]

[1]Department of Oceanography, Naval Postgraduate School, Monterey, CA, USA, [2]Institute of Oceanology, Polish Academy of Sciences, Sopot, Poland, [3]International Arctic Research Center, University of Alaska, Fairbanks, AK, USA, [4]Los Alamos National Laboratories, Los Alamos, NM, USA

Abstract Recent observations suggest that substantial phytoplankton blooms occur under sea ice on Arctic continental shelves during June and July. This is opposed to the traditional view that no significant biomass is produced in sea-ice covered waters. However, no observational estimates are available on the Arctic-wide primary production beneath sea ice. Here, using a fully coupled Arctic system model, we estimate that 63%/41% of the total primary production in the central Arctic occurs in waters covered by sea ice that is ≥50%/≥85% concentration. The total primary production there is increasing at a rate of 5.2% per decade during 1980–2018. Increased light transmission, due to the removal of sea ice, more extensive melt ponds, and thinner sea ice, is implicated as the main cause of increasing trends in primary production.

Plain Language Summary At present, there are no Arctic-wide observations and estimates of primary production beneath Arctic sea ice because it cannot be measured by satellite and is difficult to access via ship. Utilizing our state-of-the-art Arctic system model, we have quantified the primary production beneath Arctic sea ice and our findings show that the majority of production occurs in waters covered by at least 50% ice. This analysis represents a major revision to the traditional view that no significant biomass is produced in sea-ice covered waters. Our results are consistent with recent and very limited (in space and time) observational studies; however, we provide information for the entire Arctic Ocean, including increasing trends in production over the time period of 1980–2018.

Key Points:
- The majority of modeled primary production in the central Arctic is found beneath sea ice
- The annual cycle of primary production in the central Arctic peaks in June due to the under-ice fraction of production
- Primary production and photosynthetically active radiation are increasing in the central Arctic over the period 1980–2018

Correspondence to:
J. Clement Kinney,
jlclemen@nps.edu

Citation:
Clement Kinney, J., Maslowski, W., Osinski, R., Jin, M., Frants, M., Jeffery, N., & Lee, Y. J. (2020). Hidden production: On the importance of pelagic phytoplankton blooms beneath Arctic Sea ice. *Journal of Geophysical Research: Oceans*, *125*, e2020JC016211. https://doi.org/10.1029/2020JC016211

Received 10 MAR 2020
Accepted 13 JUL 2020
Accepted article online 4 AUG 2020

©2020. The Authors.
This is an open access article under the terms of the Creative Commons Attribution-NonCommercial-NoDerivs License, which permits use and distribution in any medium, provided the original work is properly cited, the use is non-commercial and no modifications or adaptations are made.

1. Introduction

Observations of pelagic phytoplankton blooms beneath Arctic sea ice are limited due to the nature of the problem. Satellite observational systems cannot detect these blooms due to the presence of sea ice. Therefore, obtaining such measurements requires the use of ship time aboard an icebreaker during spring. However, the majority of international sampling projects occur later in the season during summer, when ship travel is easier due to the annual thinning and melting of sea ice (Hill et al., 2018). Sea ice-covered pelagic phytoplankton blooms have been detected in the Arctic by limited *in situ* observations (Arrigo et al., 2012; Fortier et al., 2002; Fukuchi et al., 1989; Legendre et al., 1989); however, the prevalence and importance of these blooms to total Arctic primary production (PP) is unknown. It is believed that pelagic diatoms are the dominant phytoplankton functional type found in sea ice-covered blooms in the Western Arctic. In fact, diatoms made up over 80% of the species composition during one bloom observed in July 2011 in the northern Chukchi Sea beneath heavy sea ice (Arrigo et al., 2012). This bloom was not defined as a marginal ice zone bloom, as one might assume, but was instead observed to extend more than 100 km into the pack ice.

Numerical model results presented here were produced using the Regional Arctic System Model (RASM; please see Section 2 for a description of the model), and they provide new insights on the timing, distribution, and trends in diatom chlorophyll-*a* concentration (chl-*a*) and PP in sea ice-covered versus open waters of the Arctic Ocean over the period 1980–2018. The model results presented here have been previously compared with those of Arrigo et al. (2012) and show that the model is able to represent the location and magnitude of the observed bloom quite well, although the timing of the modeled bloom was about 2 weeks earlier than observed (Frants et al., 2020). The disparity in timing is believed to be due to a small difference in the modeled position of the ice edge as compared to the satellite-observed sea ice concentration (Frants et al., 2020).

Marine biogeochemical (BGC; mBGC) modeling is a relatively young branch of climate system science, particularly in the sea ice-covered Arctic. Early relevant work includes that of Slagstad (1985) who utilized a phytoplankton model driven by two-dimensional (2-D) physical conditions of the Barents Sea marginal ice zone. In addition, Niebauer and Smith (1989) used a 2-D biological model coupled to ice-atmosphere-ocean processes in the marginal ice zone of Fram Strait. More recent work by Jin et al. (2016) compared results among three ice-ocean-biogeochemistry models and found (their Figure 9) that ice-covered PP (defined as regions where ice concentration was >15%) ranged between 25% and 40% of the total PP north of the Arctic Circle (AC). The horizontal resolution used in this study was below the threshold that allows for eddy development in the Arctic. Jin et al. (2018) found that moving to a higher spatial resolution and adding an improved mixed layer depth scheme improved simulation of nitrate concentrations and PP, especially in areas with sharp bathymetric gradients such as along shelf breaks in the Western Arctic. Their 9-km model configuration, which produced results with the lowest biases in the Jin et al. (2018) study, is the predecessor to the updated model version used and analyzed here.

Some of the key challenges in advancing mBGC modeling have been related to the accuracy of large-scale model physics and interfacial fluxes between model components, the representation of mesoscale space and time variability, and complex biological-chemical interactions, as well as limited observational data (Doney, 1999), especially in the Arctic Ocean (Popova et al., 2012). While significant progress has been made to improve carbon cycle feedbacks and/or the iron-limited Southern Ocean modeling in Earth system models (ESMs; Ciais et al., 2013; Moore et al., 2013; Nevison et al., 2016; Popova et al., 2012), many challenges in modeling mBGC in the Arctic Ocean remain. The regional modeling approach of RASM is a compromise between the need for model complexity and high resolution versus model domain and the modern computational power presently available to address some of those challenges.

2. Methods

We utilize results from RASM to quantify the pelagic diatom chlorophyll-*a* concentration (chl-*a*) and PP in the upper 122 m (12 vertical levels) during the simulation period of 1980–2018. RASM is a high-resolution atmosphere-ice-ocean-land regional model with a domain encompassing the entire marine cryosphere of the Northern Hemisphere, including the major inflow and outflow pathways, with extensions into the North Pacific and Atlantic oceans (Figure 1). The components of RASM are the Weather Research and Forecasting (WRF) model, the variable infiltration capacity (VIC) land hydrology model, and the Los Alamos National Laboratory (LANL) Parallel Ocean Program (POP) and Sea Ice (CICE) Models. In this "fully-coupled" model, fluxes are communicated between components of the system as shown in Figure 2. The model resolution is 50 km for WRF and VIC, and 1/12° (9 km) for POP, CICE, and mBGC. RASM has been developed over the past decade, and each component, as well as the fully coupled system, has been evaluated substantially (Brunke et al., 2018; Cassano et al., 2017; DuVivier et al., 2016; Hamman et al., 2016, 2017; Jin et al., 2018; A. Roberts et al., 2015; A. F. Roberts et al., 2018). The most recent components added to this system model are ocean and sea ice biogeochemistry (mBGC), which were added in 2013 and 2016, respectively (Jeffery et al., 2020; Jin et al., 2018). In the current configuration, BGC cycling is linked with fluxes between the sea ice and pelagic ecosystem components.

The ocean BGC component is a medium-complexity Nutrients-Phytoplankton-Zooplankton-Detritus (NPZD) model (Moore et al., 2002, 2004, 2013) with a total of 24 state variables. The first 12 variables are inorganic nitrate (NO_3), inorganic silicate (SiO_3), inorganic phosphate (PO_4), ammonia (NH_4), inorganic iron (Fe), dissolved inorganic carbon (DIC), alkalinity, dissolved organic nitrogen (DON), dissolved organic phosphate (DOP), dissolved organic iron (DOFe), dissolved organic carbon (DOC), and dissolved oxygen (O_2). Eleven variables describe three phytoplankton functional groups including diatoms, small phytoplankton (flagellates), and diazotrophs, with explicit carbon, Fe, and chl-*a* pools for each category, as well as an explicit SiO_3 pool for diatoms and an implicit $CaCO_3$ pool for small phytoplankton. The final state variable is for a herbivorous zooplankton pool. Bacterial activity is implicit in the remineralization rates of nutrients and organic carbon. Additional details on the BGC model initial conditions and previous model validation efforts can be found in Jin et al. (2018).

The sea ice BGC component is part of the state-of-the-art CICE Version 6. We are using the option to vertically resolve the ice (zbgc), which allows for vertical transport and BGC processes throughout the ice

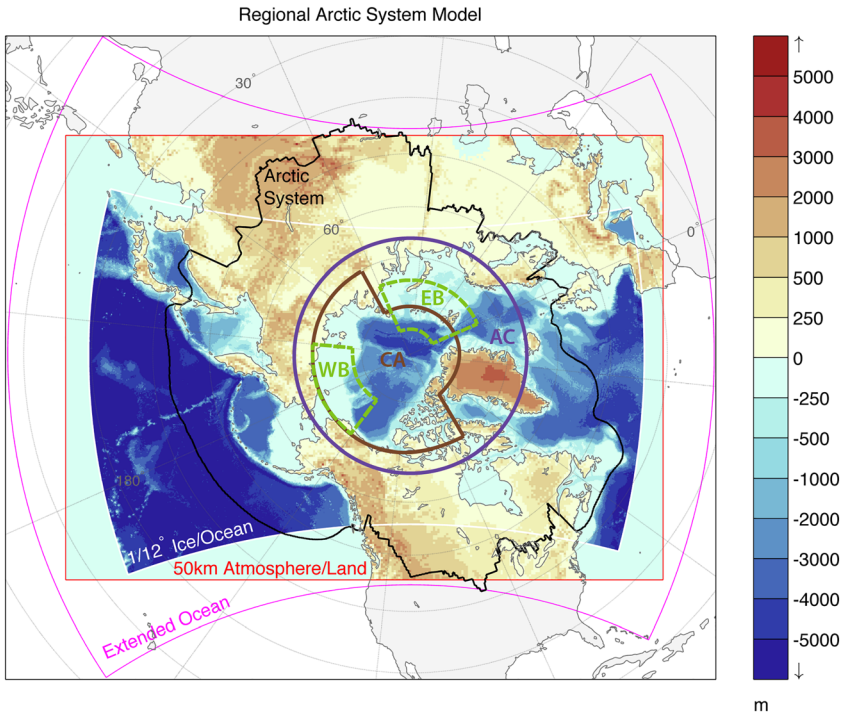

Figure 1. Model component domains, regions, and topography/bathymetry. The regions include North of the Arctic Circle (AC; 66.56°N; purple circle), the central Arctic (CA; brown line), and the western bloom and eastern bloom (WB and EB, respectively, green dashed lines). The WB and EB regions were chosen to correspond to the analysis presented in Frants et al. (2020), which showed that these locations consistently represented areas of high PP.

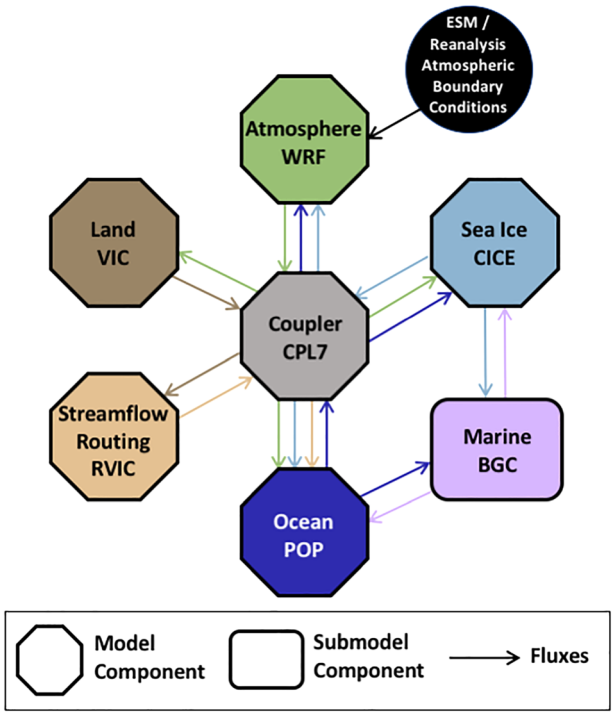

Figure 2. Wiring diagram for RASM showing model components and how fluxes are communicated among them.

column with eight layers. The model includes three algal categories (diatoms, small phytoplankton, and *Phaeocystis* sp.), two dissolved organic carbon tracers (polysaccharides and lipids), a DON tracer, NO_3, NH_4, SiO_3, dissolved Fe (FeD), dimethylsulfide (DMS), and dissolved and particulate dimethylsulfoniopropionate (DMSPd and DMSPp). Additional details on the sea ice BGC component can be found in Jeffery et al. (2020).

Coupled model simulations were run for the time period 1980–2018 after an initial 76-year spin-up integration for the physical (ocean and sea ice) components and an additional 9-year spin-up for the BGC ocean and sea ice components. Sea ice concentration is a model variable that quantifies the percentage of sea ice covering each model grid cell. A concentration of 50% means that half of the grid cell is sea ice-covered and half is sea ice-free or open ocean. In order to quantify the diatom chl-*a* beneath sea ice with a concentration of ≥50%, we (1) integrated the diatom chl-*a* over a depth of 0–122 m for each grid cell, (2) classified each model grid cell as either sea ice-covered or sea ice-free based on the concentration of sea ice present in each model grid cell, (3) summed the diatom chl-*a* in sea ice-covered grid cells only across four regions (central Arctic [CA], western bloom [WB], eastern bloom [EB], and AC). Finally, we computed the mean for the simulation time period (1980–2018) from monthly mean output (Table 1). The same process was followed for PP (including all three phytoplankton functional groups) as for diatom chl-*a*. Due to constraints on computation time and storage, we had to make use of

Table 1
Percentage of Ice-covered Pelagic Diatom Chl-a and PP that is Found in the Upper 122 m Under Various Sea Ice Concentration Thresholds

	Diatom chl-*a*				PP			
Ice concentration (%)	CA	WB	EB	AC	CA	WB	EB	AC
≥50	68.1	49.1	56.8	44.5	63.0	46.7	46.7	35.3
≥75	58.5	38.3	44.4	35.7	52.3	35.9	33.8	26.5
≥85	47.2	29.6	33.4	27.6	40.8	27.4	23.7	19.5
≥90	31.7	17.1	21.7	18.2	25.7	15.4	13.9	11.9
≥99	5.3	2.0	1.9	2.8	0.2	0.1	0.05	0.1

Note. Percentages are averages over the simulation time period (1980–2018). Regions are shown in Figure 1. Abbreviations: CA, central Arctic; WB, western bloom; EB, eastern bloom.

monthly mean output instead of daily output. A test utilizing daily output for 1 year revealed a difference of <5% between the daily-averaged and monthly-averaged PP and sea ice concentration. This small difference between time averaging (<5%) was true for all regions and ice concentration thresholds shown in Table 1.

3. Results

RASM results show between 44.5% and 68.1% of the diatom chl-*a* can be found beneath sea ice that is ≥50% in concentration, depending on the region (regions shown in Figure 1; data shown in Table 1). These numbers are a mean over the time period of 1980–2018. As we increase the sea ice concentration threshold (Table 1), the integrated ice-covered diatom chl-*a* decreases. However, ice-covered chl-*a* is still important even where sea ice is ≥90% (over 30% of the CA chl-*a* is found here).

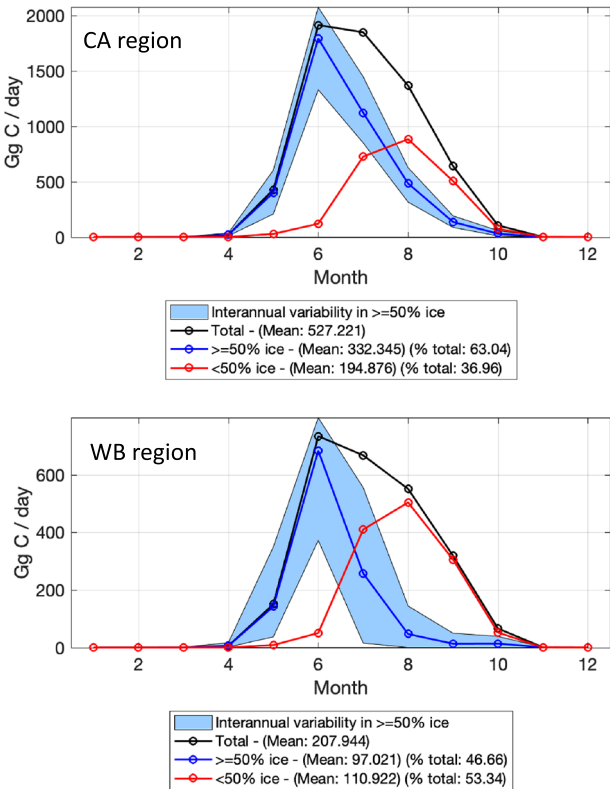

Figure 3. Mean annual cycle of PP (Gg C/d) in the CA region (upper panel) and WB region (lower panel) over the period 1980–2018. The black line represents the total; the blue line represents production in waters covered by ≥50% ice; the red line represents production in waters with <50% ice. The shaded blue area represents the interannual variability in production in waters covered by ≥50% ice.

PP was calculated as a sum from the model output variables of diatoms, small phytoplankton, and diazotrophs. Of these three, the diatom functional group contributes the vast majority of biomass and productivity (figure not shown). The percentage of PP beneath sea ice was highest in the CA region, with 63.0% occurring in waters covered by ≥50% sea ice and 52.3% in waters covered by ≥75% sea ice (Table 1). The percentage of PP beneath the sea ice continues to be important (40.8%) even in heavy ice (≥85% concentration), although the importance of ice-covered production dwindles where ice is ≥99% (0.2% of PP).

PP in the CA peaks in June according to our mean annual cycle model results (Figure 3). The vast majority of this June production is found under sea ice (blue line in Figure 3), with only a very small contribution from the open water fraction (red line). During July the under-ice production slows while the open water fraction increases. By August the open water fraction has become more important than the under-ice fraction, likely due to solar insolation and stratification of the water column; however, the total rate of production is about 500 Gg C/d slower than the June peak. Interannual variability in the under-ice production is largest in June with a range of ~700 Gg C/d. Moving to the WB region (Figure 3), we again see a peak in total production during June, which is predominantly found under ice. The open water fraction is highest in August, with a mean rate that is ~200 Gg C/d less than the June peak. The interannual variability in under-ice production is very large for the spring and summer months with a range of over 400 Gg C/d during June.

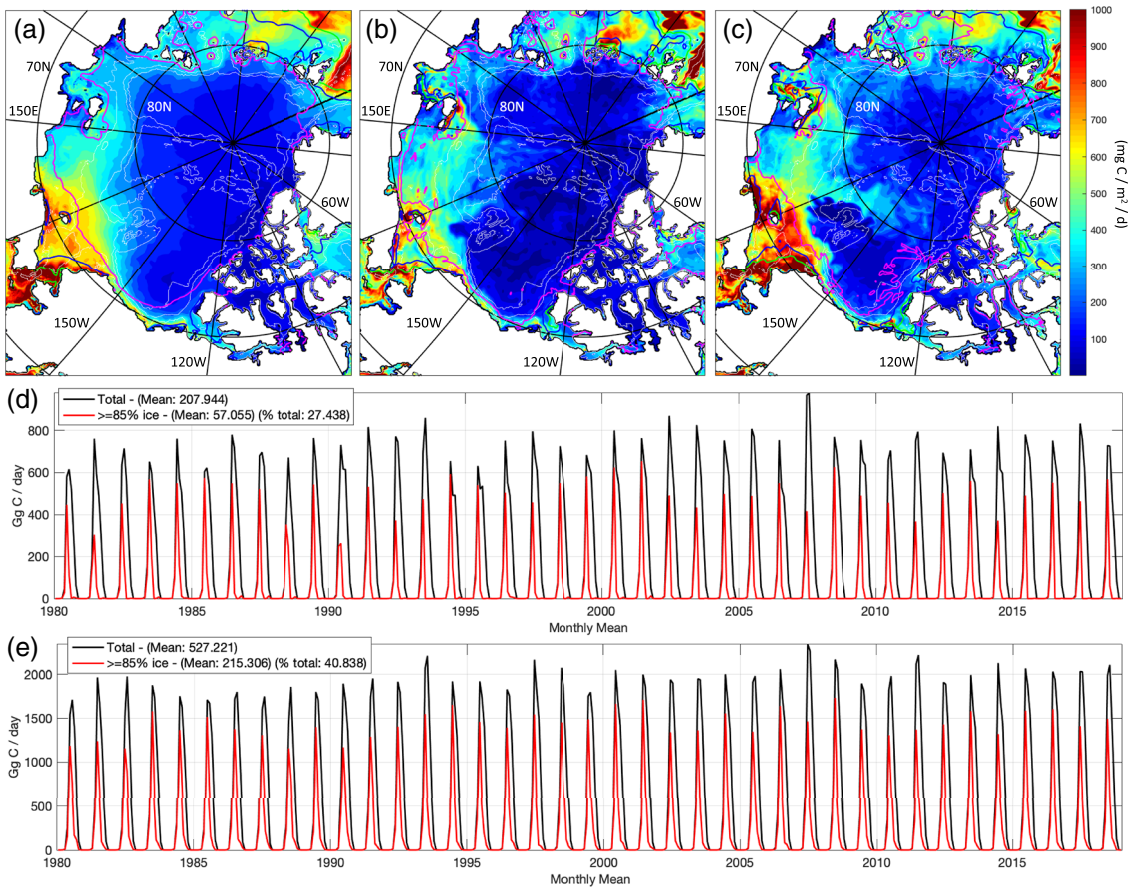

Figure 4. Upper panels: Mean primary production (mg C/m^2/d) during June averaged over 1980–2018 (a), 1980 (b), and 2011 (c). White contour lines represent bathymetry (50, 500, and 2,000 m); green, blue, and magenta contour lines represent ice concentration (15, 50, and 85%, respectively). Lower panels: Time series of monthly mean PP summed over the CA (d) and WB (e) regions (Gg C/d). Red lines represent the sum of PP in grid cells with ice concentration ≥85% and black lines represent the total PP (regardless of ice presence).

Spatially, the long-term mean June PP is highest on the Chukchi and East Siberian shelves, as well as in the Barents Sea (Figure 4a). PP during June 1980 tends to have lower values than during June 2011 in the WB region (Figures 4b and 4c). However, the area with sea ice concentration ≥50% is larger in 1980 (blue contour line), which offsets the lower magnitudes during that year and gives higher numbers for ice-covered PP.

We show that extensive ice-covered blooms have occurred frequently during spring in the past decades (Figures 4d and 4e). These results are opposed to the traditional view of low biomass beneath sea ice and consistent with recent observational findings by Arrigo et al. (2012) and Lowry et al. (2014). While the magnitudes of PP across the CA and WB tend to be lower during 1980–1998, the spatial area with heavy sea ice is greater, thereby increasing the sea ice-covered contribution to total PP.

Although the bulk of total PP in the CA occurs under sea ice, the rate of PP is lower under ice than in ice-free waters, as we would expect due to light attenuation caused by the sea ice. The regional mean PP under ≥85% ice in the CA is 48 mg C m^2/day and in areas of <85% ice the rate is 127 mg C m^2/day. The under-ice PP makes up the bulk of the total because the majority of the CA region is ice covered. So even though the rate of under-ice production is lower, there is a large area in the CA that is ice covered.

The presence of sea ice greatly reduces the photosynthetically active radiation (PAR) available to primary producers in the ocean. Table 2 shows the mean and trends of under-ice PAR in the CA region. The mean PAR in waters covered by at least 50% ice is 3.533 (W/m^2) and is 2.459 (W/m^2) in waters covered by at least 85% ice. The trends for under-ice PAR are increasing in all categories (Table 2). The PAR percent change

Table 2
Mean and Trends of Under-Ice PAR in the CA (Central Arctic) Region

Ice concentration (%)	Mean (W/m^2)	Trends and 95% confidence bounds in parenthesis (W/m^2)	Trends (percent of mean per year)	Percent change over the period 1980–2018
≥50	3.533	0.01068 (0.005666, 0.0157)	0.30	11.7
≥75	2.873	0.006966 (0.003017, 0.01091)	0.24	9.36
≥85	2.459	0.005563 (0.00226, 0.008866)	0.23	8.97
≥90	2.132	0.006165 (0.0029, 0.009429)	0.29	11.31
≥99	0.722	0.002441 (−0.005143, 0.01002)	0.34	13.26

Note. The means are for the period 1980–2018. The trends are given in absolute numbers (Column 3), as a percentage of the mean (Column 4), and as a total percent change over the simulation time period (Column 5).

over the simulation time period (1980–2018) ranges between 8.97% (waters covered by at least 85% ice) and 13.26% (for waters covered by at least 99% ice).

Figure 5 shows the modeled June PAR during 1980 (a) and 2011 (b). A magenta contour line in Figure 5 denotes the 85% sea ice concentration. PAR values in the northern Bering, Chukchi, and Beaufort seas are much higher in 2011 than in 1980 due to reduced sea ice presence. North of the 85% ice concentration line (magenta line) we also see increased PAR values during 2011 compared with 1980. In addition, the under-ice PAR is slightly higher in the northern WB region than the northern EB region. In particular, during June 2011 the under-ice PAR in the WB is up to 20 W/m^2, while it only reaches values up to 10 W/m^2 in the EB. This difference in under-ice PAR means that the WB is able to support more production due to increased light availability during late spring.

Decadal linear trends for total diatom chl-*a* and PP were computed for each region over the simulation period (1980–2018; Table 3). These trends are all increasing, with an exception of the diatom chl-*a* in the EB region. The strongest trends occur in the CA and WB regions. CA diatom chl-*a* is increasing at a rate of 3.2% of the mean per decade, and PP is increasing at a rate of 5.2% per decade. WB diatom chl-*a* is increasing at a rate of 2.3% of the mean per decade and PP is increasing at a rate of 4.3% per decade. The higher trend values for the CA and WB appear to be driven by larger declines in the sea ice area and thickness in the Western Arctic over the last several decades (modeled figures not shown; Perovich et al., 2018). In the EB region, the diatom chl-*a* is likely decreasing at a rate of −1.5% per decade, while the PP is slightly increasing at a rate of 1.0% per decade. Results from Frants et al. (2020) utilize these same model results and show that the EB region appears to be dominated by an advected phytoplankton bloom, hence less dependent on changes in the sea ice cover compared to one that is actually formed under the ice.

Realistic simulation of the sea ice cover, including area and thickness as well as the upper ocean mesoscale variability in space and time, is essential for credible simulation of mBGC processes. The ability of RASM to simulate a highly realistic sea ice cover has been documented elsewhere (Maslowski et al., 2012;

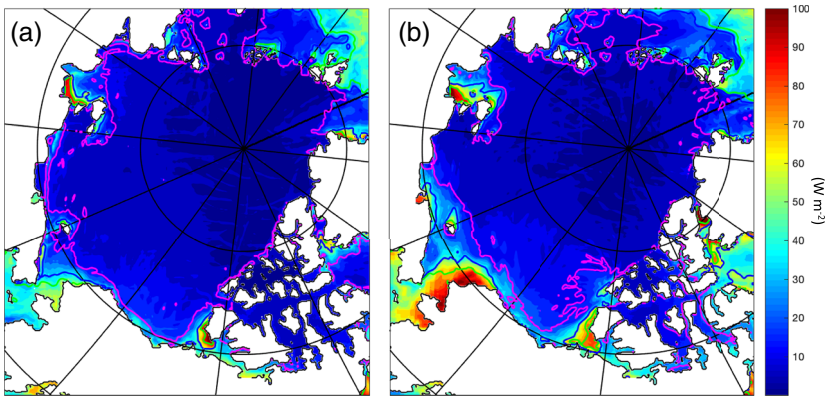

Figure 5. Ocean surface PAR during June (a) 1980 and (b) 2011. Green, blue, and magenta contour lines represent ice concentration (15%, 50%, and 85%, respectively).

Table 3
Linear Decadal Trends (and 95% Confidence Bounds in Parenthesis) in Total Diatom Chl-a (Gg/decade), Total Pp (Gg C/decade), Sea Ice Area (Million Km^2/decade), and Sea Ice Volume (Thousand Km^3/decade) Over the Simulation Period (1980–2018) for Various Regions

Quantity	CA	WB	EB	AC
Diatom chl-*a*	2.91 (1.72, 4.11)	0.836 (0.0732, 1.60)	−0.496 (−1.19, 0.199)	1.86 (0.0195, 3.71)
PP	27.6 (19.7, 35.5)	8.98 (3.59, 14.38)	1.93 (−2.25, 6.12)	33.7 (20.9, 46.5)
Sea ice area	−0.0981 (−0.135, −0.0609)	−0.0434 (−0.0640, −0.0228)	−0.0287 (−0.0510, −0.00644)	−0.183 (−0.241, −0.125)
Sea ice volume	−0.129 (−1.50, −1.07)	−0.0127 (−0.0184, −0.00705)	−0.0195 (−0.0274, −0.0116)	−0.148 (−0.172, −0.123)

Note. Regional abbreviations are defined in Figure 1.

Roberts et al., 2015, 2018). These latest RASM results using CICE Version 6 (CICE6) represent a further improvement and capability of relevance to mBGC modeling. The parameterization of melt ponds in CICE6 allows for realistic simulation of light penetration into the upper ocean as snow and sea ice begin to melt in spring and summer, which is important for spring bloom initiation (Arrigo et al., 2014; Horvat et al., 2017; Palmer et al., 2014). Linear trends in the annual mean sea ice area and thickness are all negative during the simulation period. According to RASM annual mean results, the CA region is losing 98,100 km^2 (or 1.5%) and 1.29 km^3 (or 10.8%) of sea ice area and volume per decade, respectively. The earlier and more widespread summer melt has allowed for greater light availability and, subsequently, for increased production in recent years. The areal melt has been more extensive in the western Arctic as opposed to the eastern Arctic, with a loss of 3.8% per decade in the WB region and a loss of 2.3% per decade in the EB. The changes in diatom chl-*a* concentration and PP are negatively correlated with changes in sea ice area and volume. The strongest correlations exist between sea ice area and PP ($R = -0.85$ for CA, −0.78 for WB, −0.83 for EB and −0.89 for AC; all are significant at the 90% level).

Arrigo and van Dijken (2011) estimated a total PP of 438 ± 21.5 Tg C/yr north of the AC (66.56°N) during the period 1979–1998. The modeled total PP that is found within the same region is 495 Tg C/yr averaged over a similar time period (1980–1998). It is important to note that the observed estimate is largely based on satellite information and does not include ice-covered production. Therefore, the actual total PP might be considerably higher, based on our model results shown here (Table 1). The modeled total PP averaged over the entire simulation (1980–2018) is 507 Tg C/yr in the AC region.

4. Conclusions

For the past several decades, the majority of diatom chl-*a* and PP in the CA is found in waters that are at least partially covered by sea ice, according to our pan-Arctic model results. This biological activity has largely been left out of previous estimates of total PP in the Arctic (Arrigo et al., 2014) due to immense challenges in observation, but has been hypothesized to be important (Arrigo & van Dijken, 2011). Observations indicate that enormous phytoplankton blooms can exist and even develop beneath heavy ice (Arrigo et al., 2012). Obtaining observations of phytoplankton chl-*a* and PP beneath sea ice during spring and early summer continues to be a logistical challenge. It is important to note the although the bulk of the PP occurs under sea ice, the rates of PP are lower under ice than in open water. However, the under-ice area of the CA region is substantial, making it a large habitat for primary producers. We expect that as under-ice PAR continues to increase, due to sea ice thinning and increased melt pond presence, we will see PP increase until nutrient limitation takes over.

Populations of pelagic phytoplankton found beneath sea ice make up the bulk of PP in the CA and need to be observed throughout the region, particularly during the spring and early summer, to improve understanding of their contribution to the global carbon cycle. Although the model compares well with limited measurements of an ice-covered bloom (Frants et al., 2020), more ice-covered observational data are needed to confirm the commonality of annual springtime blooms in the western and EB regions as shown by the model.

State-of-the-art pan-Arctic models with mBGC, such as the one presented here, are not currently able to simulate the extreme peaks of productivity that have been observed (Jin et al., 2016; Lee et al., 2016) and, therefore, may underestimate the total production. However, the model output presented here is very useful for determining spatial patterns and long-term trends in Arctic PP. In addition, model results are not limited

by space, time, or presence of sea ice. We believe that more realistic model representation of ocean mesoscale dynamics (e.g. eddies), which requires further increases in spatial resolution of the physical and biological model components, should help improve simulation of the large peaks and patchiness of biological variables that occur in reality. In addition, we know that the representation of clouds is an area of needed improvement in climate models (Taylor et al., 2019). Improved representation of clouds in future simulations could further enhance the model's ability to simulate more accurate PAR at the ocean's surface and, therefore, more accurate PP.

Model results presented here could serve as guidance to future field expeditions, especially if the present capability is expanded into a probabilistic prediction of sea ice-covered phytoplankton blooms at seasonal and longer time scales. As the Arctic continues on a downward trend of sea ice presence, PP continues on an upward trend. These two variables are highly correlated and are intricately linked. One of the key outstanding questions in that regard is whether the upward trend in PP will continue as the Arctic sea ice approaches seasonally ice-free conditions in summer. A second question to address in future modeling efforts is how the changing sea ice will affect the balance between phytoplankton functional types.

Data Availability Statement

Model output that was used to generate the figures and analysis in this article can be obtained (from the following website https://nps.box.com/s/ug6be32gdu7hpm49a5jarmimikq71xzr).

Acknowledgments

We acknowledge Andrew Roberts for the creation of the original Figure 1. We also thank two anonymous reviewers for their insightful comments, which improved a previous version of this article.

References

Arrigo, K. R., Perovich, D. K., Pickart, R. S., Brown, Z. W., Van Dijken, G. L., Lowry, K. E., et al. (2012). Massive phytoplankton blooms under Arctic sea ice. *Science*, *336*(6087), 1408. https://doi.org/10.1126/science.1215065

Arrigo, K. R., Perovich, D. K., Pickart, R. S., Brown, Z. W., van Dijken, G. L., Lowry, K. E., et al. (2014). Phytoplankton blooms beneath the sea ice in the Chukchi Sea. *Deep-Sea Research Part II: Topical Studies in Oceanography*, *105*, 1–16. https://doi.org/10.1016/j.dsr2.2014.03.018

Arrigo, K. R., & van Dijken, G. L. (2011). Secular trends in Arctic Ocean net primary production. *Journal of Geophysical Research*, *116*, C09011. https://doi.org/10.1029/2011JC007151

Brunke, M. A., Cassano, J. J., Dawson, N., Duvivier, A. K., Gutowski, W. J., Hamman, J., et al. (2018). Evaluation of the atmosphere-land-ocean-sea ice interface processes in the Regional Arctic System Model version 1 (RASM1) using local and globally gridded observations. *Geoscientific Model Development*, *11*(12), 4817–4841. https://doi.org/10.5194/gmd-11-4817-2018

Cassano, J. J., DuVivier, A., Roberts, A., Hughes, M., Seefeldt, M., Brunke, M., et al. (2017). Development of the Regional Arctic System Model (RASM): Near-surface atmospheric climate sensitivity. *Journal of Climate*, *30*(15), 5729–5753. https://doi.org/10.1175/JCLI-D-15-0775.1

Ciais, P., Sabine, C., Bala, G., Bopp, L., Brovkin, V., Canadell, J., et al. (2013). Carbon and other biogeochemical cycles. In T. F. Stocker, D. Qin, G.-K. Plattner, M. Tignor, S. K. Allen, J. Boschung, et al. (Eds.), *Climate Change 2013: The Physical Science Basis. Contribution of Working Group I to the Fifth Assessment Report of the Intergovernmental Panel on Climate Change* (Chap. 6, pp. 465–570). Cambridge, England: Cambridge University Press. https://doi.org/10.1017/CBO9781107415324.015

Doney, S. C. (1999). Major challenges confronting marine biogeochemical modeling. *Global Biogeochemical Cycles*, *13*(3), 705–714. https://doi.org/10.1029/1999GB900039

DuVivier, A. K., Cassano, J. J., Craig, A., Hamman, J., Maslowski, W., Nijssen, B., et al. (2016). Winter atmospheric buoyancy forcing and oceanic response during strong wind events around southeastern Greenland in the Regional Arctic System Model (RASM) for 1990–2010. *Journal of Climate*, *29*(3), 975–994. https://doi.org/10.1175/JCLI-D-15-0592.1

Fortier, M., Fortier, L., Michel, C., & Legendre, L. (2002). Climatic and biological forcing of the vertical flux of biogenic particles under seasonal Arctic Sea ice. *Marine Ecology Progress Series*, *225*, 1–16. https://doi.org/10.3354/meps225001

Frants, M., Maslowski, W., Osinski, R., Jeffery, N., Jin, M., & Clement Kinney, J. (2020). *Evaluation of under Sea-Ice Phytoplankton Blooms in the Fully-Coupled, High-Resolution Regional Arctic System Model (RASM), Preprint*. ESSOAr. https://doi.org/10.1002/essoar.10503749.1

Fukuchi, M., Watanabe, K., Tanimura, A., Hoshiai, T., Sasaki, H., Satoh, H., & Yamaguchi, Y. (1989). A phytoplankton bloom under sea ice recorded with a moored system in lagoon Saroma Ko, Hokkaido, Japan. *Proceedings of the National Institute of Polar Research (NIPR) Symposium on Polar Biology*, *2*, 9–15.

Hamman, J., Nijssen, B., Brunke, M., Cassano, J., Craig, A., DuVivier, A., et al. (2016). Land surface climate in the regional Arctic system model. *Journal of Climate*, *29*(18), 6543–6562. https://doi.org/10.1175/JCLI-D-15-0415.1

Hamman, J., Nijssen, B., Roberts, A., Craig, A., Maslowski, W., & Osinski, R. (2017). The coastal streamflow flux in the Regional Arctic System Model. *Journal of Geophysical Research: Oceans*, *122*, 1683–1701. https://doi.org/10.1002/2016JC012323

Hill, V. J., Light, B., Steele, M., & Zimmerman, R. C. (2018). Light availability and phytoplankton growth beneath arctic sea ice: Integrating observations and modeling. *Journal of Geophysical Research: Oceans*, *123*, 3651–3667. https://doi.org/10.1029/2017JC013617

Horvat, C., Jones, D. R., Iams, S., Schroeder, D., Flocco, D., & Feltham, D. (2017). The frequency and extent of sub-ice phytoplankton blooms in the Arctic Ocean. *Science Advances*, *3*(3), e1601191. https://doi.org/10.1126/sciadv.1601191

Jeffery, N., Maltrud, M., Hunke, E., Wang, S., Wolfe, J., Turner, A., et al. (2020). Investigating controls on sea ice algal production using E3SMv1.1-BGC. *Annals of Glaciology*, 1–22. https://doi.org/10.1017/aog.2020.7

Jin, M., Deal, C., Maslowski, W., Matrai, P., Roberts, A., Osinski, R., et al. (2018). Effects of model resolution and ocean mixing on forced ice-ocean physical and biogeochemical simulations using global and regional system models. *Journal of Geophysical Research: Oceans*, *123*, 358–377. https://doi.org/10.1002/2017JC013365

Jin, M., Popova, E. E., Zhang, J., Ji, R., Pendleton, D., Varpe, Ø., et al. (2016). Ecosystem model intercomparison of under-ice and total primary production in the Arctic Ocean. *Journal of Geophysical Research: Oceans*, *121*, 934–948. https://doi.org/10.1002/2015JC011183

Lee, Y. J., Matrai, P. A., Friedrichs, M. A. M., Saba, V. S., Aumont, O., Babin, M., et al. (2016). Net primary productivity estimates and environmental variables in the Arctic Ocean: An assessment of coupled physical-biogeochemical models. *Journal of Geophysical Research: Oceans*, *121*, 8635–8669. https://doi.org/10.1002/2016JC011993

Legendre, L., Ingram, R. G., & Poulin, M. (1989). Physical control of phytoplankton production under sea ice (Manitounuk Sound, Hudson Bay). *Canadian Journal of Fisheries and Aquatic Sciences*, *38*, 1385–1392. https://doi.org/10.1139/f81-185

Lowry, K. E., van Dijken, G. L., & Arrigo, K. R. (2014). Evidence of under-ice phytoplankton blooms in the Chukchi Sea from 1998 to 2012. *Deep-Sea Research Part II: Topical Studies in Oceanography*, *105*, 105–117. https://doi.org/10.1016/j.dsr2.2014.03.013

Maslowski, W., Clement Kinney, J., Higgins, M., & Roberts, A. (2012). The future of Arctic Sea ice. *Annual Review of Earth and Planetary Sciences*, *40*(1), 625–654. https://doi.org/10.1146/annurev-earth-042711-105345

Moore, J. K., Doney, S. C., Kleypas, J. A., Glover, D. M., & Fung, I. Y. (2002). An intermediate complexity marine ecosystem model for the global domain. *Deep-Sea Research Part II: Topical Studies in Oceanography*, *49*(1–3), 403–462. https://doi.org/10.1016/S0967-0645(01)00108-4

Moore, J. K., Doney, S. C., & Lindsay, K. (2004). Upper ocean ecosystem dynamics and iron cycling in a global three-dimensional model. *Global Biogeochemical Cycles*, *18*, 1–21. https://doi.org/10.1029/2004GB002220

Moore, J. K., Lindsay, K., Doney, S. C., Long, M. C., & Misumi, K. (2013). Marine ecosystem dynamics and biogeochemical cycling in the community earth system model [CESM1(BGC)]: Comparison of the 1990s with the 2090s under the RCP4.5 and RCP8.5 scenarios. *Journal of Climate*, *26*(23), 9291–9312. https://doi.org/10.1175/JCLI-D-12-00566.1

Nevison, C. D., Manizza, M., Keeling, R. F., Stephens, B. B., Bent, J. D., Dunne, J., et al. (2016). Evaluating CMIP5 ocean biogeochemistry and Southern Ocean carbon uptake using atmospheric potential oxygen: Present-day performance and future projection. *Geophysical Research Letters*, *43*, 2077–2085. https://doi.org/10.1002/2015GL067584

Niebauer, H. J., & Smith, W. O. (1989). A numerical model of mesoscale physical-biological interactions in the Fram Strait marginal ice zone. *Journal of Geophysical Research*, *94*(C11), 16,151–16,175. https://doi.org/10.1029/JC094ic11p16151

Palmer, M. A., Saenz, B. T., & Arrigo, K. R. (2014). Impacts of sea ice retreat, thinning, and melt-pond proliferation on the summer phytoplankton bloom in the Chukchi Sea, Arctic Ocean. *Deep-Sea Research Part II: Topical Studies in Oceanography*, *105*, 85–104. https://doi.org/10.1016/j.dsr2.2014.03.016

Perovich, D., Meier, W., Tschudi, M., Farrell, S., Hendricks, S., Gerland, S., et al. (2018). Sea ice. *Arctic Report Card 2018* (pp. 25–32). Washington, DC: National Oceanic and Atmospheric Administration. https://www.arctic.noaa.gov/Report-Card

Popova, E. E., Yool, A., Coward, A. C., Dupont, F., Deal, C., Elliott, S., et al. (2012). What controls primary production in the Arctic Ocean? Results from an intercomparison of five general circulation models with biogeochemistry. *Journal of Geophysical Research*, *117*, C00D12. https://doi.org/10.1029/2011JC007112

Roberts, A., Craig, A., Maslowski, W., Osinski, R., Duvivier, A., Hughes, M., et al. (2015). Simulating transient ice-ocean Ekman transport in the Regional Arctic System Model and Community Earth System Model. *Annals of Glaciology*, *56*(69), 211–228. https://doi.org/10.3189/2015AoG69A760

Roberts, A. F., Hunke, E. C., Allard, R., Bailey, D. A., Craig, A. P., Lemieux, J.-F., & Turner, M. D. (2018). Quality control for model development subject areas: Author for correspondence. *Philosophical Transactions of the Royal Society A: Mathematical, Physical and Engineering Sciences*, *376*(2129), 1–18. https://doi.org/10.1098/rsta.2017.0344

Slagstad, D. (1985). A model of phytoplankton in the marginal sea-ice zone of the Barents Sea. In J. S. Gray & M. E. Christiansen (Eds.), *Marine Biology of Polar Regions and Effects of Stress on Marine Organisms* (pp. 129–140). Hoboken, NJ: John Wiley & Sons.

Taylor, P. C., Boeke, R. C., Li, Y., & Thompson, D. W. (2019). Arctic cloud annual cycle biases in climate models. *Atmospheric Chemistry and Physics*, *19*(13), 8759–8782. https://doi.org/10.5194/acp-19-8759-2019

View publication stats